Preprints of the
9th International Symposium on Advanced Control of Chemical Processes
The International Federation of Automatic Control
June 7-10, 2015, Whistler, British Columbia, Canada

A Distributed Parameter Model for a Solid Oxide Fuel Cell: Simulating Realistic Operating Conditions

Dayadeep S. Monder * **V. Goutham Polisetty** **
Phanindra V. Jampana ** **Vinod M. Janardhanan** **

* *Department of Energy Science and Engineering,*
Indian Institute of Technology Bombay
Mumbai 400076 India (dmonder@iitb.ac.in).
** *Department of Chemical Engineering,*
Indian Institute of Technology Hyderabad
Yeddumailaram 502205 India.

Abstract: We present a detailed multiphysics model capable of simulating the dynamic behavior of a solid oxide fuel cell (SOFC). This model includes a description of all the important physical and chemical processes in a fuel cell: fluid flow, mass and heat transfer, electronic and ionic potential fields, as well as the chemical and electrochemical reactions. The resulting highly nonlinear, coupled system of differential equations is solved using a finite volume discretization. Our interest lies in simulating realistic operating conditions with the objective of high efficiency operation at high fuel utilization. While there are a number of studies in the literature that present multiphysics models for SOFCs, few have focused on simulating operating conditions that are necessary if SOFC systems are to realize their promise of high efficiency conversion of chemical energy to electrical energy. In this report we present simulation results at operating conditions that approach the required ranges of power density and overall efficiency. Our results include a) the temperature and composition profiles along a typical fuel cell in a SOFC stack, b) the dynamic response of the cell to step changes in the available input variables. Since models such as the one presented here are fairly expensive computationally and cannot be directly used for online model predictive control, one generally looks to use simplified reduced order models for control. We briefly discuss the implications of our model results on the validity of using reduced models for the control of SOFC stacks to show that avoiding operating regions where well-known degradation modes are activated is non-trivial without using detailed multiphysics models.

Keywords: physically based control relevant modeling, high efficiency operation of fuel cells, degradation risk modeling.

1. INTRODUCTION

Solid oxide fuel cells (SOFCs) have recieved increasing attention from the research community in the last 20 years. This is primarily because SOFC systems are capable of very high energy conversion efficiencies ($\eta > 50\%$, fuel to electricity) and are much more fuel-flexible than other fuel cell technologies. Thus, there is significant interest in developing mid to large scale systems that run on hydrocarbon fuels that are either fed directly to the SOFC stacks or partially reformed before they are introduced into the stacks.

Physics based models derived from first principles are key to improving the design and control of SOFC stacks and associated systems. There are a number of physically based dynamic models available in the literature for the control and optimization of SOFC cells and stacks (see Bhattacharyya and Rengaswamy (2009) and the citations within). Most of these models are lumped parameter models and only a handful (*e.g.*, Colclasure et al. (2011)) present fully coupled distributed parameter models that predict composition and temperature profiles throughout the cell/stack. One of our goals is to develop models that can be used to study SOFC cell and stack degradation modes such as anode oxidation and coke formation which are highly dependent on local conditions inside the cells. Since lumped parameter models can only compute average compositions and temperature for a cell or a stack, they cannot be used to investigate such degradation modes. Models that can predict temperature and composition profiles within the cells and stacks are key to coming up with improved designs that minimize degradation. Recently Neidhardt et al. (2013) presented a film growth model for Ni oxidation at a single point in a SOFC anode and gave rates of NiO film growth at different P_{O_2} and V_{cell}. Although Neidhardt et al. (2013) cite similar detailed SOFC models to ours and state these can be coupled to their film growth model, they do not use a detailed SOFC model in the above paper.

This paper presents a multiphysics model of an SOFC operating on reformed CH_4. The model includes a description of all reactions in the $CH_4/H_2O/H_2/CO/CO_2$ system on Ni and can thus also simulate SOFC operation using CH_4 either directly or partially reformed CH_4. The model accounts for convective transport in the flow channels, porous media diffusion in the electrodes, electrochemistry at the interface between dense electrolyte and electrodes, thermo-catalytic chemistry in the anode, and heat transport in the flow channels and the cell assembly. This model is an extension of the model given in Zhu et al. (2005) to include heat generation in the cell and heat transfer between the cell and the gas flows. The modeled cell is assumed to be made of standard SOFC materials: a porous composite Ni-YSZ (nickel - yttria stabilized zirconia) anode, a YSZ electrolyte, and a porous composite LSM-YSZ (lanthanum strontium manganate) cathode. A brief desciption of the aforementioned physico-chemical processes and resulting model components is given in Section 2. Section 3 presents some early results for temperature and composition profiles as well as transient responses to changes in system inputs. The relevance of the results to the investigation of Ni oxidation (a key anode degradation mode) is highlighted in Section 3.

2. PROBLEM FORMULATION

This section describes the model geometry, the assumptions involved, the fundamental equations, and the solution algorithm.

2.1 Geometry

The model considers a repeating unit in a co-flow solid oxide fuel cell (see Figure 1). The cell is 10 cm long, and the various layer dimensions are given in Table 1.

Table 1. Model geometry dimensions

layer	thickness
air channel	1 mm
fuel channel	1 mm
anode	750 μm
cathode	30 μm
electrolyte	25 μm

2.2 Assumptions

- Both the fuel and air gas mixtures behave as ideal gases. This is justified because of the high temperature and low pressure in SOFC operation.
- Constant pressure in the flow channels.
- The cross-section of the flow channels is small ($\sim$1 mm) and the diffusivities are high enough (*e.g.*, $D_{H_2-H_2O} \sim 1 \times 10^{-3}$ m^2/s) that the concentration gradients across the channel cross-section are neglible. Thus plug flow is a valid assumption for species transport in the channels.
- The aspect ratio L/d (where L is the length of the cell and d is the depth of the electrodes) is large for the cell assembly so that species transport in the electrodes is essentially one dimensional and perpendicular to channel flow.
- The temperature variations along the cell thickness can also be neglected due to the large aspect ratio.

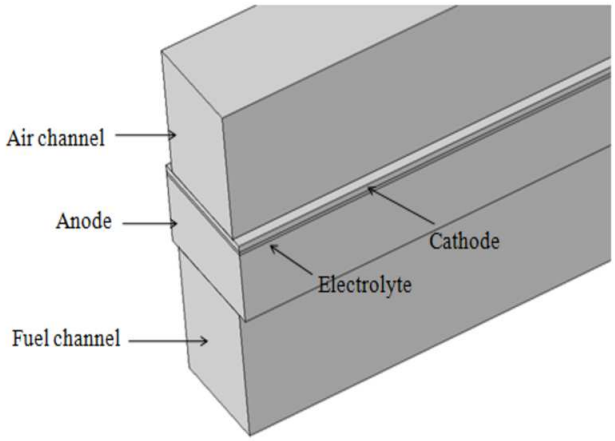

Fig. 1. Three dimensional visualization of the modelled cell.

2.3 Flow, temperature and composition in the fuel and air channels

The plug flow species transport equation for the gas mixture in the flow channel is given by Zhu et al. (2005):

$$\frac{\mathrm{d}(\rho u Y_k)}{\mathrm{d}x} = \frac{P_\mathrm{e}}{A_\mathrm{c}} J_k M_k, \quad k = 1, \ldots, N_\mathrm{g}. \tag{1}$$

where ρ is the density, u is the velocity, Y_k is the mass fraction of species k, x is the independent coordinate, P_e is the electrochemically active perimeter, A_c is the area of cross section of flow channel, J_k is the molar flux of species k, M_k is the molecular weight of species k, and N_g is the total number of gasphase species. The velocity in the channel is calculated from

$$\frac{\mathrm{d}(\rho u)}{\mathrm{d}x} = \sum_{k=1}^{N_\mathrm{g}} \frac{P_\mathrm{e}}{A_\mathrm{c}} J_k M_k, \quad k = 1, \ldots, N_\mathrm{g}. \tag{2}$$

The term on the right hand side represents the mass addition or depletion in the flow channel. In the fuel flow channel mass enters the channel due to electrochemical oxidation reactions while mass leaves the air channel due to the electrochemical reduction of O_2 to O^{2-} ions. Since the pressure is assumed to be constant in the flow channels, the density is calculated from

$$\rho = \frac{p\overline{M}}{RT}. \tag{3}$$

where $\overline{M}$ is the average molecular weight, R is the universal gas constant, and T is the temperature of the gas phase. The temperature of the gas phase is evaluated from the energy balance equation

$$\rho u c_\mathrm{p} \frac{\mathrm{d}T}{\mathrm{d}x} = \frac{4}{D_\mathrm{h}} h (T_\mathrm{s} - T), \tag{4}$$

where D_h is the hydraulic diameter, h is the heat transfer coefficient, and T_s is the temperature of the cell or membrane-electrode assembly (MEA). The heat transfer coefficient is evaluated from

$$h = \frac{Nu\ \lambda}{D_{\mathrm{h}}}. \tag{5}$$

where λ is the thermal conductivity of the gas mixture and Nu is the Nusselt number, which may be evaluated from channel flow correlations (*e.g.*, see Janardhanan and Deutschmann (2007)).

2.4 Flow, temperature and composition in the cell assembly

Unlike the governing equations for the flow channel, the governing equations for the electrodes are written in the transient form. The species transport equation in the direction perpendicular to the channel flow is given by

$$\epsilon\frac{\partial(\rho Y_k)}{\partial t} + \frac{\partial(J_k M_k)}{\partial y} = A_{\mathrm{s}}\dot{s}_k M_k, \quad k = 1, \ldots, N_{\mathrm{g}}. \tag{6}$$

where ϵ is the porosity, A_{s} is the active area per unit volume, and $\dot{s}_k$ is the rate of production of species k. Gas phase reactions are not considered because the temperature is low enough to neglect such reactions. Fuel side reactions on the Ni in the porous anode are considered using a microkinetic formulation with 21 reversible reactions among 12 adsorbed species and 6 gas species. The reader is referred to Zhu et al. (2005) for more details. The density in the electrode is given by

$$\epsilon\frac{\partial\rho}{\partial t} + \sum_{k=1}^{N_{\mathrm{g}}}\frac{\partial(J_k M_k)}{\partial y} = \sum_{k=1}^{N_{\mathrm{g}}}\dot{s}_k A_{\mathrm{s}} M_k. \tag{7}$$

The pressure within the electrodes is evaluated from the ideal gas equation Eq. 3. The molar flux of species k, J_k is evaluated according to the dusty gas model (see Zhu et al. (2005) for more details).

2.5 Cell assembly (solid phase) heat balance

Since the temperature variations across the MEA is neglected due to the large aspect ratio L/d, the energy balance equation for the MEA is given by

$$\rho_{\mathrm{s}} c_{\mathrm{s}}\frac{\partial T_{\mathrm{s}}}{\partial t} - \frac{\partial}{\partial x}\left(\lambda_{\mathrm{s}}\frac{\partial T_{\mathrm{s}}}{\partial x}\right) = Q. \tag{8}$$

where ρ_{s} is the average density, c_{s} is the average specific heat, and λ_{s} is the average thermal conductivity of the MEA. The source term Q is given by

$$Q = -\frac{A_{\mathrm{c}}}{P_{\mathrm{e}} H_{\mathrm{mea}}}\sum_{k=1}^{N_{\mathrm{g}}}\frac{\mathrm{d}(\dot{m} h_k Y_k)}{\mathrm{d}x} - \frac{VI}{H_{\mathrm{mea}}}. \tag{9}$$

where $\dot{m}$ is the mass flux, H_{mea} is the total thickness of the anode, cathode, and electrolyte, and h_k is the specific enthalpy of species k. The first term on the right hand side of Eq. 9 represents the two contributions under adiabatic conditions. i) the enthalpy change due to chemical reaction and ii) enthalpy change due to heat exchange with MEA in the flow channels. If there is no heat exchange between the MEA and the flow channels, then this term solely represents the reaction heat, which is assumed to be liberated in the electrodes.

2.6 Boundary conditions

At the interface between the electrodes and the dense electrolyte, the species fluxes are given by

$$J_k = \pm\frac{i}{n_{\mathrm{e}} F}, \tag{10}$$

where i is the current density, n_{e} is the number of electrons transferred during the charge transfer reaction, and F is the Faraday's constant. The current density i for the both the anode and cathode is calculated using modified Butler-Volmer equations that are functions of the local overpotential, composition and temperature first presented in Zhu et al. (2005). The reader is referred to Janardhanan and Deutschmann (2007) for more details on these functions. The fluxes are zero for species which do not take part in the electrochemical reactions. At the exit of the flow channels, the boundary conditions are given by:

$$\left.\frac{\mathrm{d}Y_k}{\mathrm{d}x}\right|_{x=L} = 0 \quad \left.\frac{\mathrm{d}T}{\mathrm{d}x}\right|_{x=L} = 0 \quad \left.\frac{\mathrm{d}u}{\mathrm{d}x}\right|_{x=L} = 0 \tag{11}$$

The inlet boundary conditions are specified by the inlet concentrations, velocity, temperature and pressure for the fuel and air streams (Table 1). The inlet fuel composition used here is for reformed natural gas as given in Newby and Keairns (2011).

Table 2. Inlet gas phase conditions

	fuel	air
mole fractions	H_2 51%	O_2 21%
	CH_4 0.06%	N_2 79%
	CO 19%	
	H_2O 23%	
	CO_2 6.2%	
temperature	650 ^{o}C	650 ^{o}C
pressure	1 atm	1 atm
velocity	19 cm/s	1.5 m/s

2.7 Solution algorithm

The channel flow governing equations are solved as a space marching problem which requires the species flux J_k at the interface between the flow channel and electrode for each axial position. The evaluation of these fluxes using the dusty gas equation requires the species composition within the electrodes. Therefore, for each axial position the governing equations for the electrodes are time integrated until steady state. The species composition within the flow channel and the species flux at the interface between the electrode and dense electrolyte serves as the boundary condition for solving these equations. The energy balance equation for the MEA, Eq. 8 is decoupled from the rest of the governing equations. For each time step of Eq. 8, one full march is performed in the flow direction.

2.8 Fuel utilization, cell efficiency and the thermodynamics of Ni oxidation

The net efficiency of any fuel cell is given by

$$\eta = \frac{(VI)_{cell}}{\sum_i \dot{n}_i \Delta H_i} \tag{12}$$

where V_{cell} and I_{cell} are the operating cell voltage and current, $\dot{n}_i$ is the molar flow rate and ΔH_i is the enthalpy of combustion of fuel species i.

Fuel utilization is given by

$$U_f = \frac{I_{cell}}{F \sum_i n_{e,i} \dot{n}_i} \tag{13}$$

where the numerator is the actual current produced and $n_{e,i}$ is the number of electrons generated upon electrochemical oxidation of species i. The denominator is the current that would be generated if all the fuel species were electrochemically oxidised.

The Ni in the anode microstructure can be oxidized to NiO through reaction 14. This reaction becomes thermodynamically favourable at points where the local P_{H_2O}/P_{H_2} ratio increases beyond a well defined threshold as shown below.

$$Ni + H_2O \rightarrow NiO + H_2 \tag{14}$$

The Gibbs free energy for the Ni oxidation reaction above is given by

$$\Delta G = \Delta G^0 + RT \log(Q) \tag{15}$$

where ΔG^0 is the standard state Gibbs free energy at temperature T and Q is given by

$$Q = \Pi_i a_i^{\nu_i} \tag{16}$$

which is the product of the activities (a_i) of the participating chemical species raised to the power the respective stoichiometric coefficients (ν_i). For the Ni oxidation reaction considered here

$$Q = \frac{a_{NiO} a_{H_2}}{a_{Ni} a_{H_2O}} = \frac{P_{H_2}}{P_{H_2O}} \tag{17}$$

as the solid species activity is taken as unity and the ideal gas law applies.

For a reaction to be favourable, $\Delta G < 0$, or

$$\Delta G = \Delta G^0 + RT \log(Q) < 0 \tag{18}$$
$$-RT \log(K) + RT \log(Q) < 0 \tag{19}$$
$$RT \log(Q/K) < 0 \tag{20}$$
$$Q/K < 1 \text{ or } K/Q > 1 \tag{21}$$

where $K = \exp(-\Delta G^0/RT)$. Applying this to reaction 14, it is apparent that nickel oxidation is thermodynamically favourable wherever $K/Q > 1$. Because Q decreases along the fuel channel/anode from the inlet to the exit, one gets the highest value for K/Q at the fuel exit.

3. RESULTS AND DISCUSSION

The model described above is used to simulate the operation of a planar SOFC and some of the results are presented here. The operating conditions are defined by the inlet conditions given in Table 2 and the operating cell voltage V_{cell} and the results below describe cell operation at specified steady state conditions as well as the transients seen when step changes are introduced in V_{cell}.

3.1 Temperature, current, composition profiles

Figure 2 shows three plots for fuel composition, current density and temperature along the length of the cell at $V_{cell} = 0.7$ V. This is the nominal operating point for this study and the average current density $i_{av} = 0.227$ A/cm^2, the cell temperature is $T_{av} = 771\,^o$C, and the fuel utilization $U_f = 81.1\%$. Since this is a co-flow cell running on reformate with very little methane, it is not surprising that the temperature rises uniformly from the inlet to the outlet. The gas phase temperature approaches the solid phase temperature very quickly in the initial section of the cell and tracks the solid temperature along the cell; the fuel side temperature rises faster than the air side temperature because the fuel flow-rate is lower. As seen in the composition profiles, the H_2 mole fraction rises initially before falling steadily all the way to the exit. The initial rise in y_{H_2} is because of the water gas shift reaction that uses the CO in the fuel to convert H_2O to H_2 and CO_2. The peak in the current density is interesting, the initial rise is due to the rise in cell temperature and the subsequent fall in i_{av} is because of the decrease in y_{H_2}. The air side composition (not shown) does not have a major effect as the O_2 utilization is only 14%.

Because detailed composition and temperature profiles are obtained from the model results, this model can predict which operating conditions can lead to *local* conditions that favour degradation modes such as anode oxidation and coking. We show how we use this model to predict the conditions under which Ni oxidation becomes favourable in section 3.3.

3.2 Response to step change in cell voltage

Figure 3 shows the response of the fuel utilization, average current density and average cell temperature when V_{cell} is changed from 0.7 V to 0.6 V at $t = 300$ seconds. The current responds instantaneously and a distinct but slight overshoot is seen in the first 100 seconds or so. The average cell temperature responds much more slowly, taking about 200 seconds to reach the new (higher) steady state value. These differences in timescales are well known from earlier studies (see Bhattacharyya and Rengaswamy (2009); Colclasure et al. (2011)). The substantial increase in U_f from 81% to 99% due to the change in operating voltage is noteworthy.

3.3 High fuel utilization

Figure 4 shows how the steady state fuel composition, temperature, and current density changes along the cell at three cell voltages. The average current density increases from 227 mA/cm^2 to 285 mA/cm^2 when V_{cell} changes from 0.7 V to 0.6 V. A subsequent drop to 0.5 V offers a negligible increase in i_{av} to 287 mA/cm^2. However, as seen in Figure 4, the distribution of current density changes dramatically for these changes in cell voltage as the fuel utilization approaches 1 ($U_f = 99.75\%$ at $V_{cell} = 0.5$ V). The fuel starvation in the anode that leads to these skewed $i(x)$ distributions is also readily apparent in Figure 4. The outlet H_2 mole fraction drops from 9.4% at 0.7 V, to 0.4% at 0.6 V, and further to 0.1% at 0.5 V. Roughly half of the cell does not generate any appreciable current at 0.5 V because of fuel starvation.

Operating at high fuel utilization is desirable because higher values of U_f translate to lesser fuel wastage since the fuel exhaust is usually combusted to supply additional

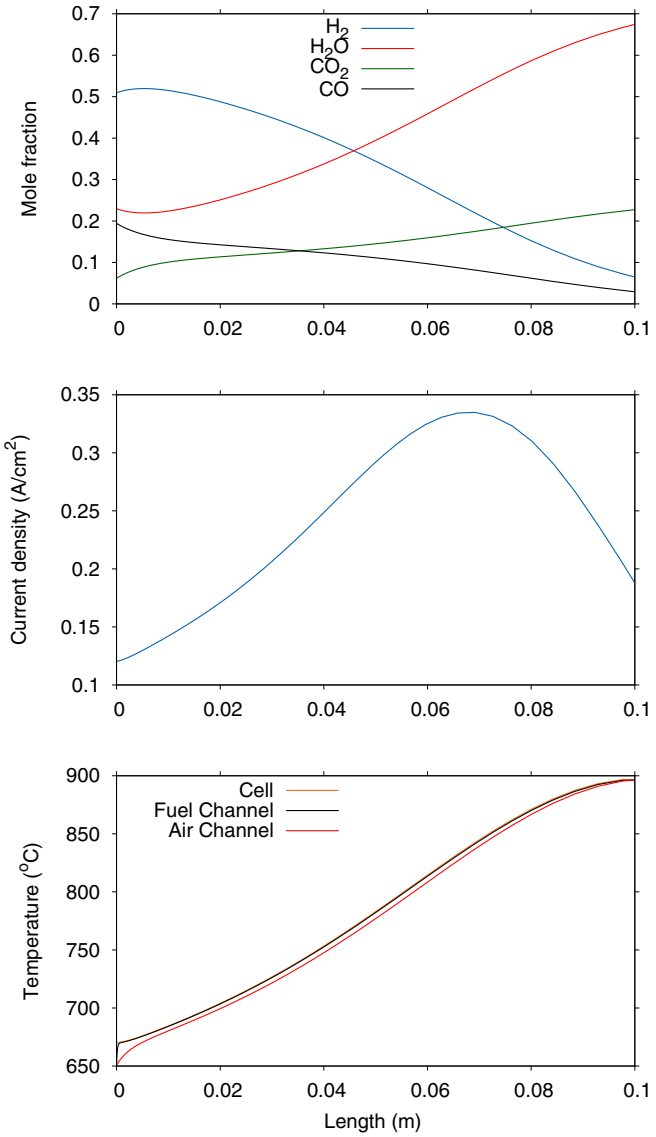

Fig. 2. Steady state composition, current density, and temperatures along the length of the cell at 0.7 V.

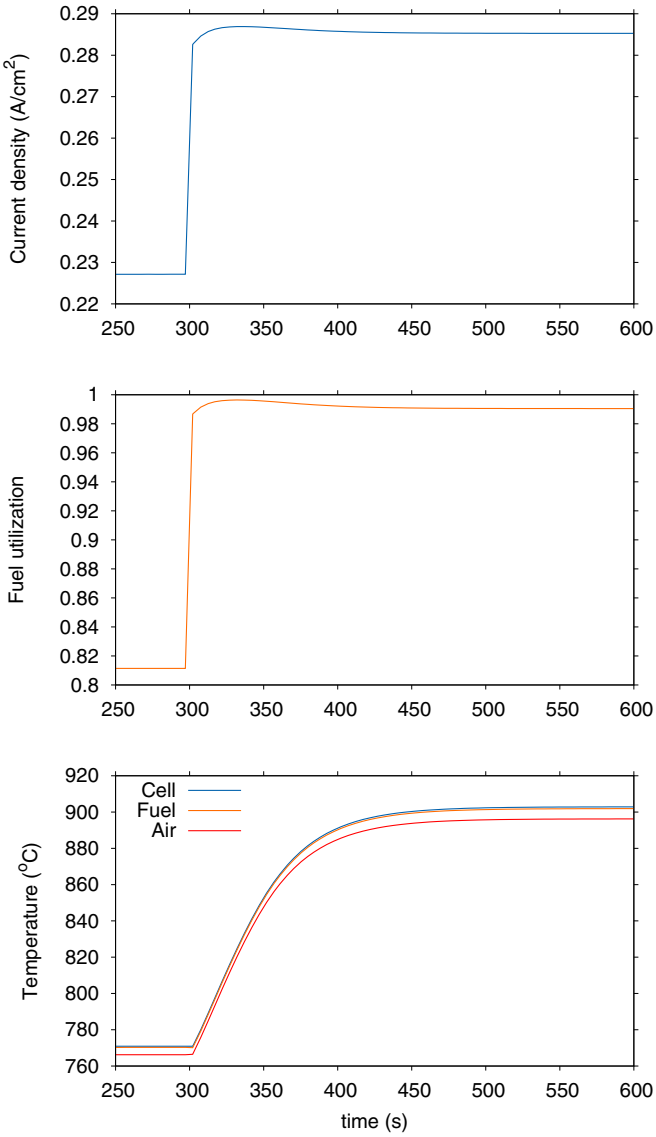

Fig. 3. Transient response of the cell to a step in cell voltage from 0.7 V to 0.6 V.

heating for the stack. A high U_f should also lead to a higher fuel cell efficiency and the maximum possible U_f is coupled to the cell voltage as shown in Zhu and Kee (2006). However, operation at high fuel utilization carries the risk of damaging the anode microstructure through the Ni redox cycling degradation mechanism (see Fouquet et al. (2003); Neidhardt et al. (2013) and references therein).

Figure 5 plots U_f, efficiency η, and K/Q in the cell for a simulation with a sequence of voltage steps of 0.1 V from 0.7 V down to 0.5 V. As seen in the bottom plot, K/Q at the fuel exit for $V_{cell} = 0.6$ V and lower is greater than 1 and thus Ni oxidation is favourable at the exit of the anode under these conditions. It is instructive to note that $U_f > 99\%$ at this point. As the voltage increases, the current density and U_f decrease, while K/Q at the fuel exit below 1. According to the above preliminary simulations for the planar SOFC cell as defined by the model parameters presented here, the fuel utilization must be kept below $\sim 99\%$ to avoid oxidation of the Ni in the anode. However, $U_F \sim 99\%$ is considered very severe operation and further work is required to see if operating zones exist that might risk Ni oxidation at significantly less severe conditions. The efficiency of the cell examined here increases from 43% at 0.7 V to 46.4% at 0.6 V but then drops to 39% at 0.5 V. Ongoing work is focusing on finding an operating window where the efficiency is higher and on examining design modifications that can improve efficiency.

4. CONCLUSIONS

We present a detailed multiphysics model for an SOFC and use it to simulate severe operating conditions that can trigger well known degradation modes. In the early results presented here, the model capabilities are illustrated by plotting steady state profiles along the cell as well as transients due to step changes in cell voltage. A

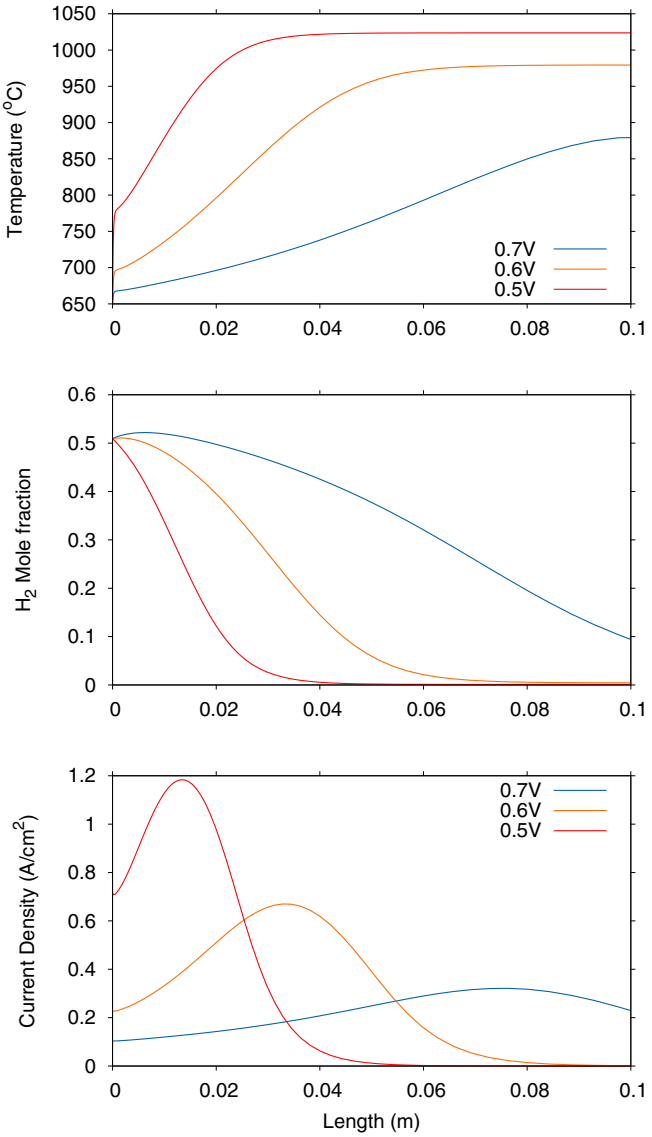

Fig. 4. Steady state composition, current density, and temperature along the length of the cell at different V_{cell}.

thermodynamic metric is presented that is then used to check whether or not Ni oxidation is favourable in the anode. As the next logical extension, we want to use this model to identify safe operating regions for a SOFC. This would be an important step towards identifying operating condition constraints.

Our ultimate goal is to design appropriate state observers and model predictive controllers for SOFC stacks. This work highlights the challenge of avoiding a degradation mechanism whose prediction requires detailed knowledge of local conditions in the cell. This is a key problem that need to be overcome in order to successfully use reduced models for SOFCs (e.g., lumped parameter models where local compositions and temperature are not computed).

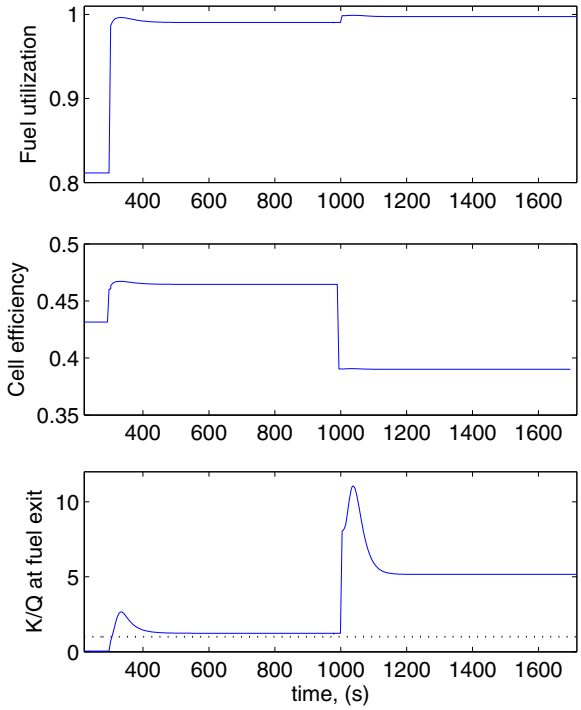

Fig. 5. Transient response of the cell to a sequence of steps in cell voltage from 0.7 V to 0.5 V.

REFERENCES

Bhattacharyya, D. and Rengaswamy, R. (2009). A review of solid oxide fuel cell (SOFC) dynamic models. *Industrial & Engineering Chemistry Research*, 48(13), 6068–6086.

Colclasure, A.M., Sanandaji, B.M., Vincent, T.L., and Kee, R.J. (2011). Modeling and control of tubular solid-oxide fuel cell systems. I: Physical models and linear model reduction. *Journal of Power Sources*, 196(1), 196 – 207.

Fouquet, D., Muller, A.C., Weber, A., and Ivers-Tiffee, E. (2003). Kinetics of oxidation and reduction of Ni/YSZ cermets. *Ionics*, 9, 103–108.

Janardhanan, V.M. and Deutschmann, O. (2007). Numerical study of mass and heat transport in solid-oxide fuel cells running on humidified methane. *Chemical Engineering Science*, 62, 5473.

Neidhardt, J., Kee, R.J., and Bessler, W.G. (2013). Electrode Reoxidation in Solid-Oxide Cells: Detailed Modeling of Nickel Oxide Film Growth. *ECS Transactions*, 57(1), 2573.

Newby, R. and Keairns, D. (2011). Analysis of Natural Gas Fuel Cell Plant Configurations. National Energy Technology Laboratory report DOE/NETL-2011/1486.

Zhu, H. and Kee, R.J. (2006). Thermodynamics of SOFC efficiency and fuel utilization as functions of fuel mixtures and operating conditions. *Journal of Power Sources*, 161, 957–964.

Zhu, H., Kee, R.J., Janardhanan, V.M., Deutschmann, O., and Goodwin, D.G. (2005). Modeling Elementary Heterogeneous Chemistry and Electrochemistry in Solid-Oxide Fuel Cells. *Journal of The Electrochemical Society*, 152(12), A2427.